

ARTICLE OPEN

Correlators in simultaneous measurement of non-commuting qubit observables

Juan Atalaya¹, Shay Hacohe-Gourgy^{2,3,4}, Leigh S. Martin^{2,3}, Irfan Siddiqi^{2,3} and Alexander N. Korotkov¹

One of the hallmarks of quantum mechanics is the impossibility of simultaneous measurement of non-commuting observables with projective measurements. This, however, can be circumvented by using continuous quantum measurements. Here we investigate the temporal correlations of the output signals of detectors continuously and simultaneously measuring the qubit observables σ_z and $\sigma_z \cos\varphi + \sigma_x \sin\varphi$, for various angles φ . Using the quantum Bayesian formalism, we obtain analytical expressions for the correlators, which we find to be in good agreement with those obtained from experimentally measured output signals. The agreement is particularly good for cross-correlators, even at times shorter than the cavity modes decay time. We further discuss how the correlators can be applied for parameter estimation, and use them to infer a small residual qubit Hamiltonian arising from calibration inaccuracy in the experimental data. Our work opens up new possibilities to perform quantum metrology based on temporal correlations of measured data.

npj Quantum Information (2018)4:41 ; doi:10.1038/s41534-018-0091-1

INTRODUCTION

Continuous quantum measurements (CQMs) have become a unique platform to explore fundamental aspects of quantum phenomena and have potential applications to quantum information science. They have been discussed theoretically in various contexts (e.g.,^{1–10}), and in the past decade superconducting qubits have become the main experimental system for the realization of CQMs.^{11–17} CQMs are shedding new light on our understanding of the quantum measurement process, and there is also a growing interest in CQM applications, including quantum feedback,^{13,16,18–20} rapid state purification,²¹ preparation of entangled states,^{22–24} and continuous quantum error correction.^{25,26}

While a simultaneous measurement of non-commuting observables is impossible with instantaneous projective measurements, nothing theoretically forbids such a measurement using CQMs. (This is so because a CQM can be regarded as a series of infinitesimally weak quantum measurements, and partial measurements of non-commuting observables become commuting with each other in the limit of infinitesimally weak strength.) Aside from new physics, such a protocol may open up new areas of applications, inaccessible to projective measurements. The theoretical discussion of a simultaneous measurement of incompatible observables has a long history.^{27–30} For the measurement of non-commuting observables of a qubit, statistics of time-integrated detector outputs and fidelity of state monitoring directly via time-integrated outputs has been analyzed in ref. ³¹. The evolution of the qubit state due to simultaneous measurement of incompatible variables has been described theoretically in ref. ³², and has been recently demonstrated experimentally in ref. ³³.

In this work, we focus on the temporal correlations of the output signals from two linear detectors measuring continuously and simultaneously the qubit observables σ_z and $\sigma_\varphi \equiv \sigma_z \cos\varphi + \sigma_x$

$\sin\varphi$, where σ_x and σ_z are the Pauli matrices and φ is an angle between the two measurement directions on the Bloch sphere (Fig. 1). The experimental setup is described in detail in ref. ³³; it is based on a Rabi-rotated physical qubit, which is measured stroboscopically³⁴ using symmetric sideband pumping of a coupled resonator, so that σ_z and σ_φ for an effective rotating-frame qubit are being measured. Description of such a measurement based on the theory of quantum trajectories^{8,9,35,36} has been developed in ref. ³³. In this work we will use a simpler approach based on quantum Bayesian theory.^{10,37–39} The quantum Bayesian description of the rotating-frame experiment³³ is developed in Supplementary Note 1.

We will also show that the considered correlators can be used as a sensitive tool for parameter estimation. This scheme is different from conventional quantum metrology schemes (e.g., see ref. ⁴⁰ and references therein) because it is not necessary to initialize the qubit state; in fact, the considered correlators are insensitive to the initial state even before the steady state is formed. Furthermore, the continuous measurement capability may enable monitoring of correlators in real time to perform parameter estimation of slowly time-varying parameters. Access to two different measurement channels (corresponding to σ_z and σ_φ) also enhances the parameter estimation capability by circumventing the ubiquitous problem of spurious slow fluctuations of the measurement signals offset, affecting mainly self-correlators but not much cross-correlators, since noise in different amplifiers is usually not correlated. We will demonstrate such correlator-based parameter estimation scheme by finding a small frequency mismatch, $\tilde{\Omega}_R$, between the frequency of stroboscopic measurement and the Rabi-oscillations frequency, using the cross-correlator for $\varphi = \pi/2$.

¹Department of Electrical and Computer Engineering, University of California, Riverside, CA 92521, USA; ²Quantum Nanoelectronics Laboratory, Department of Physics, University of California, Berkeley, CA 94720, USA and ³Center for Quantum Coherent Science, University of California, Berkeley, CA 94720, USA

Correspondence: Juan Atalaya (jatalayachavez@ece.ucr.edu)

⁴Present address: Department of Physics, Technion, Haifa 3200003, Israel

Received: 27 September 2017 Revised: 3 August 2018 Accepted: 7 August 2018

Published online: 04 September 2018

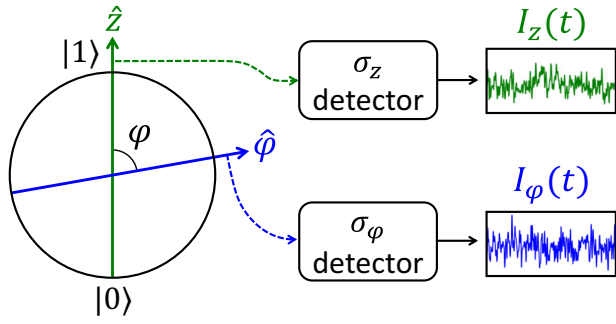


Fig. 1 We consider the simultaneous continuous measurement of qubit observables σ_z and σ_φ , which differ by an angle φ on the Bloch sphere, and calculate time-correlators for the output signals $I_z(t)$ and $I_\varphi(t)$ resulting from this measurement

The goals of this paper are (i) calculation of the time-correlators for the output signals measuring σ_z and σ_φ , and their comparison with experimental data, and (ii) demonstration that these correlators may be a useful tool for sensitive parameter estimation in an experiment. The considered correlators are also important in the analysis of quantum error detection and correction based on simultaneous measurement of non-commuting operators.⁴¹ We note that the analyzed output signal correlators are different from qubit-state correlators.⁴²

RESULTS

Quantum Bayesian theory

A simultaneous continuous measurement (Fig. 1) of the qubit observables σ_z and σ_φ by two linear⁴³ (non-switching) detectors produces noisy output signals $I_z(t)$ and $I_\varphi(t)$, respectively.^{32,37–39}

$$I_z(t) = \text{Tr}[\sigma_z \rho(t)] + \sqrt{\tau_z} \xi_z(t), \quad (1)$$

$$I_\varphi(t) = \text{Tr}[\sigma_\varphi \rho(t)] + \sqrt{\tau_\varphi} \xi_\varphi(t), \quad (2)$$

where $\rho(t)$ is the qubit density matrix and τ_z and τ_φ are the “measurement” (collapse) times needed for an informational signal-to-noise ratio of 1 for each channel. Note the chosen normalization for I_z and I_φ . In the Markovian approximation, the noises ξ_z and ξ_φ are uncorrelated, white, and Gaussian with two-time correlators

$$\langle \xi_z(t) \xi_z(t') \rangle = \langle \xi_\varphi(t) \xi_\varphi(t') \rangle = \delta(t - t') \quad (3)$$

and $\langle \xi_z(t) \xi_\varphi(t') \rangle = 0$. The qubit state is characterized in the Bloch-sphere representation as $\rho(t) \equiv [1 + x(t)\sigma_x + y(t)\sigma_y + z(t)\sigma_z]/2$. The experimental method of simultaneous measurement of σ_z and σ_φ for the effective qubit is rather involved (see Methods and ref. 33); however, its theoretical description can be based on the standard quantum Bayesian approach for the circuit QED measurement. Note that the measured operator “direction” φ is determined by a phase shift between the applied sideband tones, so parameters of the σ_φ -measurement channel do not depend on φ . Each of the two channels uses a separate phase-sensitive amplifier, with the amplified quadrature determined by the phase of the local oscillator (parametric pumping). Here we assume that in each channel, the optimal (informational) quadrature is amplified, so that the qubit evolution due to measurement is not affected by the phase backaction related to fluctuations in the orthogonal (non-informational) quadrature.^{35–39} Then there is only the quantum informational backaction, which for measurement of σ_z and σ_φ is described^{32,37–39} by the evolution equations (in the Itô

interpretation, see Supplementary Note 1)

$$\dot{x} = -\Gamma_z x - \Gamma_\varphi \cos \varphi (x \cos \varphi - z \sin \varphi) - \tau_z^{-1/2} x z \xi_z - \tau_\varphi^{-1/2} [x z \cos \varphi - (1 - x^2) \sin \varphi] \xi_\varphi, \quad (4)$$

$$\dot{y} = -(\Gamma_z + \Gamma_\varphi) y - \tau_z^{-1/2} y z \xi_z - \tau_\varphi^{-1/2} y [z \cos \varphi + x \sin \varphi] \xi_\varphi, \quad (5)$$

$$\dot{z} = \Gamma_\varphi \sin \varphi (x \cos \varphi - z \sin \varphi) + \tau_z^{-1/2} (1 - z^2) \xi_z + \tau_\varphi^{-1/2} [(1 - z^2) \cos \varphi - x z \sin \varphi] \xi_\varphi. \quad (6)$$

Here Γ_z and Γ_φ are the ensemble dephasing rates due to measurement, so that the quantum efficiencies^{37–39} for the two channels are $\eta_z = 1/(2\tau_z\Gamma_z)$ and $\eta_\varphi = 1/(2\tau_\varphi\Gamma_\varphi)$. In the experiment $\eta_z \approx 0.49$ and $\eta_\varphi \approx 0.41$ (note that η_φ is a characteristic of the measurement channel and therefore does not depend on φ).

Equations (4)–(6) describe evolution of the effective qubit due to measurement only. We also need to add terms due to unitary evolution and due to decoherence not related to measurement. We assume the Hamiltonian $H = \hbar \tilde{\Omega}_R \sigma_y / 2$, describing Rabi oscillations about y -axis with frequency $\tilde{\Omega}_R$. In the experiment, $\tilde{\Omega}_R = \Omega_R - \Omega_{rf}$ is a small (kHz-range) undesired mismatch between the Rabi frequency Ω_R of the physical qubit and rotating frame frequency Ω_{rf} defined by detuning of sideband pumps,³³ see Supplementary Note 1. Decoherence of the effective qubit arises from the decoherence of the physical qubit, which is characterized (in the laboratory frame) by energy relaxation time T_1 and dephasing time T_2 [the pure dephasing rate is then $T_{pd}^{-1} = T_2^{-1} - (2T_1)^{-1}$; note that T_1^{-1} may have a significant contribution from qubit hybridization with leaking resonator, i.e., the Purcell effect]. To find decoherence of the effective (Rabi-rotating-frame) qubit, we need to average physical decoherence over fast rotations $\Omega_R \gg T_2^{-1}$. As derived in Supplementary Note 1, the corresponding decoherence of the effective qubit (with added unitary evolution) is

$$\dot{x} = \tilde{\Omega}_R z - \gamma x, \quad \dot{y} = -T_2^{-1} y, \quad \dot{z} = -\tilde{\Omega}_R x - \gamma z, \quad (7)$$

$$\gamma = (T_1^{-1} + T_2^{-1})/2, \quad (8)$$

Evolution of the effective qubit is described by adding terms from Eqs. (4)–(6) and (7).

Correlators

Our goal is to calculate the two-time correlators, $K_{ij}(\tau)$, for the output signals,

$$K_{ij}(\tau) \equiv \langle I_j(t_1 + \tau) I_i(t_1) \rangle, \quad \tau > 0, \quad i, j \in \{z, \varphi\}. \quad (9)$$

Self- and cross-correlators correspond to $i=j$ and $i \neq j$, respectively. The averaging in Eq. (9) is over an ensemble of measurements with the initial qubit state ρ_{in} prepared at time $t_{in} \leq t_1$. We will see, however, that somewhat surprisingly, the result does not depend on ρ_{in} , t_{in} , and t_1 (even during initial non-steady-state regime), so Eq. (9) can also be understood as averaging over time t_1 . Note that this statement is correct only because of unital (symmetric) evolution in Eq. (7). We assume that the parameters describing strength of measurement, decoherence, and unitary evolution in Eqs. (4)–(7) do not change with time. By assuming $\tau > 0$, we avoid considering the trivial zero-time contribution to the self-correlators, $\Delta K_{ii}(\tau) = \tau \delta(\tau)$.

As shown in Supplementary Note 2, calculation of the correlators from Eqs. (1)–(7) is equivalent to the following recipe:⁴⁴ we replace an actual continuous measurement at the (earlier) time moment t_1 with a projective measurement of σ_{ii} , so that the measurement result $I_i(t_1)$ is ± 1 with probability $\{1 \pm \text{Tr}[\sigma_i \rho(t_1)]\}/2$, and the qubit state collapses correspondingly to the eigenstate $|1_i\rangle$ or $|0_i\rangle$ of σ_i ($\sigma_i|1_i\rangle = |1_i\rangle$, $\sigma_i|0_i\rangle = -|0_i\rangle$). We emphasize that this recipe does not assume a steady-state measurement process and does not assume a unital evolution. The recipe gives the

correlator

$$K_{ij}(\tau) = \text{Tr}[\sigma_j \rho_{\text{av}}(t_1 + \tau | 1_i)] (1 + \text{Tr}[\sigma_i \rho(t_1)]) / 2 - \text{Tr}[\sigma_j \rho_{\text{av}}(t_1 + \tau | 0_i)] (1 - \text{Tr}[\sigma_i \rho(t_1)]) / 2, \quad (10)$$

where $\rho_{\text{av}}(t_1 + \tau | 1_i)$ is the ensemble-averaged density matrix at time $t_1 + \tau$ with the initial condition $\rho_{\text{av}}(t_1 | 1_i) = |1_i\rangle\langle 1_i|$; similarly, $\rho_{\text{av}}(t_1 + \tau | 0_i)$ starts with $\rho_{\text{av}}(t_1 | 0_i) = |0_i\rangle\langle 0_i|$. The evolution of ρ_{av} is given by Eqs. (4)–(7) without noise, $\xi_z = \xi_\varphi = 0$ (because of the Itô form), so that

$$\dot{x}_{\text{av}} = -\Gamma_z x_{\text{av}} - \Gamma_\varphi \cos \varphi (x_{\text{av}} \cos \varphi - z_{\text{av}} \sin \varphi) + \tilde{\Omega}_R z_{\text{av}} - \gamma x_{\text{av}}, \quad (11)$$

$$\dot{y}_{\text{av}} = -(\Gamma_z + \Gamma_\varphi) y_{\text{av}} - T_2^{-1} y_{\text{av}}, \quad (12)$$

$$\dot{z}_{\text{av}} = \Gamma_\varphi \sin \varphi (x_{\text{av}} \cos \varphi - z_{\text{av}} \sin \varphi) - \tilde{\Omega}_R x_{\text{av}} - \gamma z_{\text{av}}. \quad (13)$$

These equations have an analytical solution presented in Supplementary Note 2 (note that the evolution of the y -coordinate is not important in our analysis). Thus we obtain the following correlators (alternative methods for the derivation are also discussed in Supplementary Note 2):

$$K_{zz}(\tau) = \frac{1}{2} \left[1 + \frac{\Gamma_z + \cos(2\varphi)\Gamma_\varphi}{\Gamma_+ - \Gamma_-} \right] e^{-\Gamma_+ \tau} + \frac{1}{2} \left[1 - \frac{\Gamma_z + \cos(2\varphi)\Gamma_\varphi}{\Gamma_+ - \Gamma_-} \right] e^{-\Gamma_- \tau}, \quad (14)$$

$$K_{z\varphi}(\tau) = \frac{(\Gamma_z + \Gamma_\varphi) \cos \varphi + 2\tilde{\Omega}_R \sin \varphi}{2(\Gamma_+ - \Gamma_-)} (e^{-\Gamma_- \tau} - e^{-\Gamma_+ \tau}) + \frac{\cos \varphi}{2} (e^{-\Gamma_- \tau} + e^{-\Gamma_+ \tau}), \quad (15)$$

$$\Gamma_\pm = \frac{\Gamma_z + \Gamma_\varphi \pm \left[\Gamma_z^2 + \Gamma_\varphi^2 + 2\Gamma_z \Gamma_\varphi \cos(2\varphi) - 4\tilde{\Omega}_R^2 \right]^{1/2}}{2} + (T_1^{-1} + T_2^{-1})/2. \quad (16)$$

Because of the rotational symmetry, the results for the correlators $K_{\varphi\varphi}(\tau)$ and $K_{\varphi z}(\tau)$ can be obtained from Eqs. (14) and (15) by exchanging $\Gamma_z \leftrightarrow \Gamma_\varphi$ and $\varphi \rightarrow -\varphi$. The rotational symmetry also makes the correlators insensitive to a y -rotation in both measurement directions, $z \rightarrow \varphi_{\text{addr}}$, $\varphi \rightarrow \varphi + \varphi_{\text{addr}}$, by any angle φ_{addr} .

We emphasize that the obtained correlators do not depend on the qubit state $\rho(t_1)$ and therefore on ρ_{in} and t_{in} (this property would not hold in the presence of phase backaction or non-unital evolution). We also emphasize that the correlators depend on Γ_z and Γ_φ , but do not depend on τ_z and τ_φ and therefore on the quantum efficiencies η_z and η_φ . Physically, this is because non-ideal detectors can be thought of as ideal detectors with extra noise at the output.^{37–39} Since the extra noises are uncorrelated and have short (zero) correlation time, they only affect the zero-time self-correlators $K_{ij}(0)$.

Let us discuss some special cases for the results (14)–(16). (i) At small times, $\tau \rightarrow +0$, we obtain correlators

$$K_{zz}(+0) = 1, K_{z\varphi}(0) = K_{\varphi z}(0) = \cos \varphi. \quad (17)$$

(ii) For $|\varphi| \ll 1$ and sufficiently small T_2^{-1} and $\tilde{\Omega}_R$, we have Zeno pinning near the states $|0\rangle$ and $|1\rangle$ with rare jumps between them with equal rates Γ_{jump} . This produces cross-correlator⁴⁵ $K_{z\varphi}(\tau) \approx \exp(-2\Gamma_{\text{jump}}\tau)$ with jump rates

$$\Gamma_{\text{jump}} = \frac{\varphi^2 \Gamma_z \Gamma_\varphi + \tilde{\Omega}_R^2}{2(\Gamma_z + \Gamma_\varphi)} + (T_1^{-1} + T_2^{-1})/4. \quad (18)$$

(iii) In the case $\tilde{\Omega}_R = T_1^{-1} = T_2^{-1} = 0$, we have full correlation for $\varphi = 0$, $K_{z\varphi}(\tau) = K_{zz}(\tau) = 1$, full anticorrelation for $\varphi = \pi$, $K_{z\varphi}(\tau) = -K_{zz}(\tau) = -1$, and no correlation for $\varphi = \pi/2$, $K_{z\varphi}(\tau) = 0$, while $K_{zz}(\tau) = e^{-\Gamma_\varphi \tau}$ and $K_{\varphi\varphi}(\tau) = e^{-\Gamma_z \tau}$. (iv) In the case $\tilde{\Omega}_R = 0$, the cross-correlator is symmetric, $K_{z\varphi}(\tau) = K_{\varphi z}(\tau)$, for any φ .

Comparison with experimental results

Experimental data have been taken in the same way as in ref.³³ (see also Methods). Experimental parameters correspond to well-separated frequency scales, as needed for the theoretical results, $(T_1^{-1}, T_2^{-1}, |\tilde{\Omega}_R|) \ll (\Gamma_z, \Gamma_\varphi) \ll (\kappa_z, \kappa_\varphi) \ll \Omega_R$, with $T_1 = 60 \mu\text{s}$, $T_{2,\text{Ramsey}} = 30 \mu\text{s}$ ($T_{2,\text{echo}} = 40 \mu\text{s}$), $\Gamma_z^{-1} = \Gamma_\varphi^{-1} = 1.3 \mu\text{s}$, damping rates of the two measurement resonator modes $\kappa_z/2\pi = 4.3 \text{ MHz}$ and $\kappa_\varphi/2\pi = 7.2 \text{ MHz}$, and $\Omega_R \approx \Omega_{\text{rf}} = 2\pi \times 40 \text{ MHz}$. For this work we use 11 values for the angle φ between the Bloch-sphere directions of simultaneously measured qubit observables: $\varphi_n = n\pi/10$, with integer n between 0 and 10. While φ_n is determined by well-controlled phases of applied microwaves,³³ the effective φ includes a small correction $\delta\varphi = (\kappa_\varphi - \kappa_z)/2\Omega_R \approx 0.036$ (see Supplementary Note 1), so that $\varphi = \varphi_n + \delta\varphi$. We have used about 200,000 traces per angle for the output signals $\tilde{I}_z(t)$ and $\tilde{I}_\varphi(t)$, each with $5 \mu\text{s}$ duration and 4 ns sampling interval. The traces are selected by heralding the ground state of the physical qubit at the start of a run and checking that the transmon qubit is still within the two-level subspace after the run (this procedure eliminates about 15% of traces). The recorded signals $\tilde{I}_i(t)$ are linearly related to the normalized signals $I_i(t)$ in Eqs. (1) and (2) as $\tilde{I}_i(t) = (\Delta\tilde{I}_i/2) I_i(t) + \tilde{I}_i^{\text{off}}$, where responses $\Delta\tilde{I}_i$ have been calibrated using ensemble-averaged $\langle \tilde{I}_i(t) \rangle$ (see details in Supplementary Note 3), giving in arbitrary units $\Delta\tilde{I}_z = 4.0$ and $\Delta\tilde{I}_\varphi = 4.4$. The offsets \tilde{I}_i^{off} are approximately zeroed individually for each trace by measuring the non-rotating physical qubit after each run. Additional offset removal, $|\tilde{I}_i^{\text{off}}| \approx 0.15\text{--}0.20$, for all traces with the same φ is done using $\langle \tilde{I}_i(t) \rangle$, see Supplementary Note 3. For calculating the correlators, we average over the ensemble of $\sim 200,000$ traces and additionally average over time t_1 in Eq. (9) within the $0.5 \mu\text{s}$ range $1 \mu\text{s} \leq t_1 \leq 1.5 \mu\text{s}$ (first $1 \mu\text{s}$ is not used to avoid transients in the experimental procedure, and longer averaging reduces the range for τ ; we also used averaging over $1 \mu\text{s}$ duration with similar results). Note that in the experiment the applied microwave phases in the two measurement channels actually correspond to angles $\pm\varphi_n/2$; however, because of rotational symmetry, we still label the first measured operator as σ_z and the second operator as σ_φ . Also note that we use subscripts z and φ in various notations (\tilde{I}_i , κ_i , etc.) simply to distinguish the first (“ z ”) and second (“ φ ”) measurement channels.

Figure 2a shows the agreement between the theory and the experimental data, where the solid lines show the symmetrized cross-correlator $[K_{z\varphi}(\tau) + K_{\varphi z}(\tau)]/2$ calculated from the experimental traces for 11 values of the angle φ , while the dashed lines correspond to the theoretical result, Eq. (15). For the analytics we used $\tilde{\Omega}_R = 0$; however, there is practically no dependence on $\tilde{\Omega}_R$ for the symmetrized cross-correlator, since the dependence comes only via Eq. (16). Note that because of the Markovian assumption, our theory is formally valid only for $\tau \gtrsim \kappa_i^{-1} \sim 30 \text{ ns}$; however, the experimental results agree with the theory even at $\tau < \kappa_i^{-1}$ (experimental curves do not show any extra features in this range, and they are also not expected theoretically). Figure 2b shows the same symmetrized cross-correlator at $\tau = 0$ as a function of φ . The agreement between the theory ($\cos \varphi$, line) and the experiment (crosses) is also very good. Note a minor discrepancy between the theory and experimental results in Fig. 2a for $\varphi \approx \pi$, while there is no discrepancy at $\varphi \approx 0$; the physical difference between these two cases stems from different effective initial states (see Supplementary Note 3), so that we expect the largest contribution from transients for $\varphi \approx \pi$.

The self-correlator $K_{zz}(\tau)$ as a function of τ is shown in Fig. 2c for 11 values of φ (results for $K_{\varphi\varphi}$ are similar). The agreement between the theory (dashed lines) and experiment (solid lines) is in general good, except for small τ (discussed below). A significant discrepancy at relatively long τ for values of φ close to $\pi/2$ is probably caused by slow variations in time of the signal offsets \tilde{I}_i^{off} ,

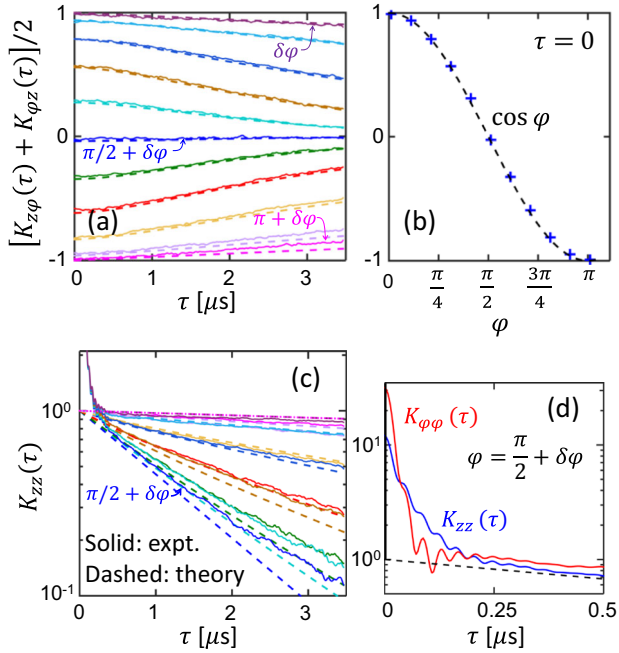


Fig. 2 Comparison between normalized experimental and theoretical correlators for the detector output signals. We used 11 angles between the measurement axes: $\varphi = \varphi_n + \delta\varphi$ where $\varphi_n = n\pi/10$, $n = 0, 1, \dots, 10$ and $\delta\varphi \approx 0.036$. Solid and dashed lines in all panels correspond to experimental and analytical results, respectively. **a** The symmetrized cross-correlator $[K_{z\varphi}(\tau) + K_{\varphi z}(\tau)]/2$ for 11 values of φ , from $n=0$ (top) to $n=11$ (bottom). **b** The crosses show φ -dependence of experimental cross-correlators from **a** at $\tau=0$, while the dashed line, $\cos\varphi$, corresponds to Eq. (17). **c** The self-correlator $K_{zz}(\tau)$ for 11 values of φ [$n=0$ and 10 at the top, $n=5$ at the bottom, the same colors as in **a**]. **d** Deviation of experimental self-correlators (for $\varphi_n = \pi/2$) from the theory at small τ due to finite bandwidth of amplifiers and filters; the thick black line at the left illustrates the theoretical δ -function

so that they are different from trace to trace and cannot be fully removed. The corresponding slight increase of the correlators become especially visible when K_{zz} is small (because of the logarithmic scale), i.e., for φ close to $\pi/2$ and long τ . Note that the lines in Fig. 2c come in pairs, corresponding to angles φ_n and $\pi - \varphi_n$. The separation of the analytical lines in the pairs is due to $\delta\varphi$, while separation of experimental lines is smaller, probably indicating a smaller value of $\delta\varphi$ (partial compensation could be due to imperfect phase matching of applied microwaves or their dispersion in the cable).

Looking at the experimental self-correlators $K_{zz}(\tau)$ and $K_{\varphi\varphi}(\tau)$ at small τ for $\varphi_n = \pi/2$ (Fig. 2d), we see that in contrast to the theoretical results, there is a very significant increase of $K_{ij}(\tau)$ at $\tau \lesssim 0.1 \mu\text{s}$. The discrepancy is due to the assumption of delta-correlated noise in our theory, while in the experiment the amplifying chain has a finite bandwidth (the Josephson parametric amplifiers have a half-bandwidth of 3.6 MHz and 10 MHz for σ_z and σ_φ channels, respectively), and the output signals $I_i(t)$ are also passed through analog filters with a quite sharp cutoff at ~ 25 MHz (this cutoff produces clearly visible oscillations with ~ 40 ns period). Therefore, the theoretical delta-function contribution $\tau_i \delta(\tau)$ to $K_{ij}(\tau)$ becomes widened in experiment. As shown in Supplementary Note 4, it is interesting to note that, somewhat counterintuitively, a finite bandwidth of measurement resonator modes does not produce a contribution to $K_{ij}(\tau)$ at $0 < \tau \lesssim \kappa_i^{-1}$ when $\Gamma_i \ll \kappa_i$ ($\kappa_z^{-1} \approx 37$ ns, $\kappa_\varphi^{-1} \approx 22$ ns). This can be understood by considering a resonator without a qubit; then a finite bandwidth κ_i does not affect the amplified delta-correlated vacuum noise, so that only classical fluctuations of the resonator field (e.g., due to

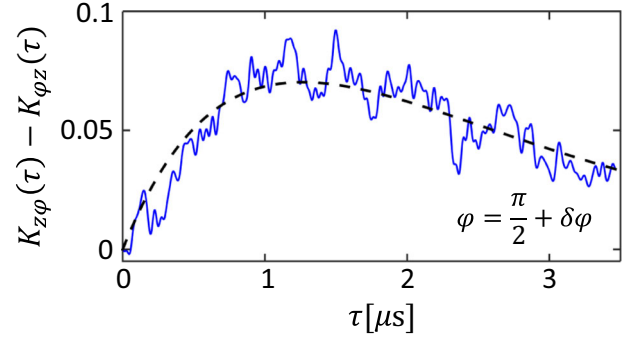


Fig. 3 Estimation of the residual Rabi frequency $\tilde{\Omega}_R$ from the antisymmetrized cross-correlator $K_{z\varphi}(\tau) - K_{\varphi z}(\tau)$. Solid line shows experimental results for $\varphi_n = \pi/2$, while dashed line represents Eq. (19) with the fitted value $\tilde{\Omega}_R/2\pi = 12$ kHz. Averaging over $\sim 200,000$ experimental traces produces a clearly-visible difference signal, though with a significant noise

parameter fluctuations or elevated resonator temperature) will produce output fluctuations with $2/\kappa_i$ time scale. We have checked that the lines in Fig. 2d do not contain noticeable exponential contributions with decay time of $2/\kappa_i$ (small expected contributions with amplitude on the order of Γ_i/κ_i are below experimental accuracy, see Supplementary Note 4). Note that there is no contribution from the amplifier noise at small τ in Fig. 2a because the noises in the two amplifiers are uncorrelated.

Estimation of residual $\tilde{\Omega}_R$

We now show that the antisymmetrized cross-correlator is a useful tool and can be used to estimate small residual Rabi oscillations frequency $\tilde{\Omega}_R$ in the experiment. From Eq. (15) we find

$$K_{z\varphi}(\tau) - K_{\varphi z}(\tau) = \frac{2\tilde{\Omega}_R \sin\varphi}{\Gamma_+ - \Gamma_-} (e^{-\Gamma_-\tau} - e^{-\Gamma_+\tau}). \quad (19)$$

Since in the case $|\tilde{\Omega}_R| \ll \Gamma_{z,\varphi}$ we can neglect $\tilde{\Omega}_R$ in Eq. (16) for Γ_{\pm} , Eq. (19) gives a direct way to find $\tilde{\Omega}_R$ from the experimental antisymmetrized cross-correlator. The solid line in Fig. 3 shows $K_{z\varphi}(\tau) - K_{\varphi z}(\tau)$ from the experimental data for $\varphi = \pi/2$. Fitting this dependence on τ with Eq. (19) (dashed line), we find the value $\tilde{\Omega}_R/2\pi \approx 12$ kHz, which is within the experimentally expected range of frequency mismatch between Ω_R and Ω_{rf} . Note that the overall shapes of the solid and dashed lines agree well with each other. Estimation of $\tilde{\Omega}_R$ via the antisymmetrized cross-correlation is a very sensitive method and can be used to further reduce $|\tilde{\Omega}_R|$ in an experiment, in which a direct measurement of 40 MHz Rabi oscillations with a few kHz accuracy is a difficult task.

DISCUSSION

Using the quantum Bayesian theory for a simultaneous measurement of non-commuting qubit observables, we obtained analytical results for the self- and cross-correlators of the output signals from the measurement. Their comparison with experimental results shows a very good agreement. The correlators can be used for sensitive parameter estimation, in particular, to estimate and eliminate the mismatch between the Rabi oscillations and the sideband frequency shift used for measurement.

Our theoretical method and results can be applied to a range of related problems. In particular, in subsystem error detection/correction codes operated with continuous measurements,⁴¹ the error syndrome is based on correlators from measurement of a set of non-commuting observables. Therefore, the analysis of

correlators is necessary for logical error analysis as well as for diagnosis of spurious dynamics of gauge qubits and deviations of monitored observables from intended observables. Our method can also be extended to multi-time correlators⁴⁶ and to experimental systems with phase backaction. Another possible application is to exploit continuous measurements to track slow variations of Rabi frequencies due to $1/f$ noise. It may also be possible to stabilize the Rabi frequencies by quantum feedback¹³ based on cross-correlators from several measurement channels.

METHODS

Experimental setup

The experimental setup is the same as the one used in the experiment,³³ where full details can be found. For clarity we briefly describe the experimental apparatus for simultaneously applying and controlling two measurement observables. We use a transmon qubit placed inside an aluminum cavity, such that it is dispersively coupled to the two lowest modes of the cavity. The cavity has two outputs, each primarily coupled to a different mode. The outputs of these modes are amplified using two lumped-element Josephson parametric amplifiers (LJPA) operated in phase sensitive mode. Each mode is then used to measure an observable of the qubit, as described below. The apparatus is cooled to 30 mK inside a dilution refrigerator.

We drive Rabi oscillations $\Omega_R/2\pi = 40$ MHz on the qubit by applying a resonant microwave tone modulated by an arbitrary waveform generator. In the frame rotating with Ω_R , this produces an effective low frequency qubit. To couple the effective qubit to the cavity modes for measurement, we apply a pair of microwave sidebands to each mode. The sidebands are detuned above and below the two cavity modes by Ω_R , which leads to a resonant interaction between the qubit Rabi oscillations and the mode. This coupling may be understood as a stroboscopic measurement of the qubit oscillations. The relative phase of the sidebands determines which quadrature of the qubit oscillations is measured. This coupling causes the cavity mode state to displace in a way that depends on the state of the qubit. We couple to the internal cavity field using a small antenna that protrudes into the cavity, allowing read out the cavity state as described above. Quantum trajectory reconstructions are validated using post-selection and tomographic measurements.

DATA AVAILABILITY

All relevant data can be obtained from the authors upon request.

ACKNOWLEDGEMENTS

We thank Justin Dressel and Andrew Jordan for useful discussions. The work was supported by ARO Grant no. W911NF-15-1-0496. L.S.M. acknowledges support from the National Science Foundation (NSF) Graduate Fellowship Grant no. 1106400. All statements of fact, opinion or conclusions contained herein are those of the authors and should not be construed as representing the official views or policies of ARO, NSF or the US Government.

AUTHOR CONTRIBUTIONS

J.A. and A.N.K. performed the theoretical analysis. S.H.-G., L.S.M. and I.S. contributed with the experiment realization. J.A. analysed the experimental correlators and made the comparison with analytical results. J.A. and A.N.K. wrote the manuscript. All authors discussed and reviewed the final version of the manuscript. All work was carried out under supervision of A.N.K. and I.S.

ADDITIONAL INFORMATION

Supplementary information accompanies the paper on the *npj Quantum Information* website (<https://doi.org/10.1038/s41534-018-0091-1>).

Competing interests: The authors declare no competing interests.

Publisher's note: Springer Nature remains neutral with regard to jurisdictional claims in published maps and institutional affiliations.

REFERENCES

1. Kraus, K. *States, effects and operations: fundamental notions of quantum theory*. (Springer: Berlin, 1983).
2. Caves, C. M. Quantum mechanics of measurements distributed in time. A path-integral formulation. *Phys. Rev. D* **33**, 1643 (1986).
3. Menskii, M. B. Decoherence and the theory of continuous quantum measurements. *Phys. Usp.* **41**, 923 (1998).
4. Belavkin, V. P. Quantum stochastic calculus and quantum nonlinear filtering. *J. Multivar. Anal.* **42**, 171 (1992).
5. Braginsky, V. B. & Khalili, F. Ya *Quantum measurement*. (Cambridge University Press, Cambridge, UK, 1992).
6. Aharonov, Y., Albert, D. Z. & Vaidman, L. How the result of a measurement of a component of the spin of a spin-1/2 particle can turn out to be 100. *Phys. Rev. Lett.* **60**, 1351 (1988).
7. Dalibard, J., Castin, Y. & Mølmer, K. Wave-function approach to dissipative processes in quantum optics. *Phys. Rev. Lett.* **68**, 580 (1992).
8. Carmichael, H. J. *An open systems approach to quantum optics*. (Springer: Berlin, 1993).
9. Wiseman, H. M. & Milburn, G. J. Quantum theory of field-quadrature measurements. *Phys. Rev. A* **47**, 642 (1993).
10. Korotkov, A. N. Continuous quantum measurement of a double dot. *Phys. Rev. B* **60**, 5737 (1999).
11. Katz, N. et al. Coherent state evolution in a superconducting qubit from partial-collapse measurement. *Science* **312**, 1498 (2006).
12. Palacios-Laloy, A. et al. Experimental violation of a Bell's inequality in time with weak measurement. *Nat. Phys.* **6**, 442 (2010).
13. Vijay, R. et al. Stabilizing Rabi oscillations in a superconducting qubit using quantum feedback. *Nature* **490**, 77 (2012).
14. Hatridge, M. et al. Quantum back-action of an individual variable-strength measurement. *Science* **339**, 178 (2013).
15. Murch, K. W., Weber, S. J., Macklin, C. & Siddiqi, I. Observing single quantum trajectories of a superconducting quantum bit. *Nature* **502**, 211 (2013).
16. de Lange, G. et al. Reversing quantum trajectories with analog feedback. *Phys. Rev. Lett.* **112**, 080501 (2014).
17. Campagne-Ibarcq, P. et al. Observing interferences between past and future quantum states in resonance fluorescence. *Phys. Rev. Lett.* **112**, 180402 (2014).
18. Wiseman, H. M. & Milburn, G. J. Quantum theory of optical feedback via homodyne detection. *Phys. Rev. Lett.* **70**, 548 (1993).
19. Ruskov, R. & Korotkov, A. N. Quantum feedback control of a solid-state qubit. *Phys. Rev. B* **66**, 041401 (2002).
20. Sayrin, C. et al. Real-time quantum feedback prepares and stabilizes photon number states. *Nature* **477**, 73 (2011).
21. Jacobs, K. How to project qubits faster using quantum feedback. *Phys. Rev. A* **67**, 030301(R) (2003).
22. Ruskov, R. & Korotkov, A. N. Entanglement of solid-state qubits by measurement. *Phys. Rev. B* **67**, 241305(R) (2003).
23. Risté, D. et al. Deterministic entanglement of superconducting qubits by parity measurement and feedback. *Nature* **502**, 350 (2013).
24. Roch, N. et al. Observation of measurement-induced entanglement and quantum trajectories of remote superconducting qubits. *Phys. Rev. Lett.* **112**, 170501 (2014).
25. Ahn, C., Doherty, A. C. & Landahl, A. J. Continuous quantum error correction via quantum feedback control. *Phys. Rev. A* **65**, 042301 (2002).
26. Sarovar, M., Ahn, C., Jacobs, K. & Milburn, G. J. Practical scheme for error control using feedback. *Phys. Rev. A* **69**, 052324 (2004).
27. Arthurs, E. & Kelly, J. L. On the simultaneous measurement of a pair of conjugate observables. *Bell Syst. Tech. J.* **44**, 725 (1965).
28. Busch, P. Indeterminacy relations and simultaneous measurements in quantum theory. *Int. J. Theor. Phys.* **24**, 63 (1985).
29. Stenholm, S. Simultaneous measurement of conjugate variables. *Ann. Phys.* **218**, 233 (1992).
30. Jordan, A. N. & Büttiker, M. Continuous quantum measurement with independent detector cross correlations. *Phys. Rev. Lett.* **95**, 220401 (2005).
31. Wei, H. & Nazarov, Yu. V. Statistics of measurement of noncommuting quantum variables: Monitoring and purification of a qubit. *Phys. Rev. B* **78**, 045308 (2008).
32. Ruskov, R., Korotkov, A. N. & Mølmer, K. Qubit state monitoring by measurement of three complementary observables. *Phys. Rev. Lett.* **105**, 100506 (2010).
33. Hacohe-Gourgy, S. et al. Quantum dynamics of simultaneously measured non-commuting observables. *Nat. (Lond.)* **538**, 491 (2016).
34. Averin, D. V. Quantum nondemolition measurements of a qubit. *Phys. Rev. Lett.* **88**, 207901 (2002).
35. Wiseman, H. M. & Milburn, G. J. *Quantum measurement and control* (Cambridge Univ. Press, Cambridge, UK, 2010).
36. Gambetta, J. et al. Quantum trajectory approach to circuit QED: quantum jumps and the Zeno effect. *Phys. Rev. A* **77**, 012112 (2008).

37. Korotkov, A. N. Selective quantum evolution of a qubit state due to continuous measurement. *Phys. Rev. B* **63**, 115403 (2001).
38. Korotkov, A.N. Quantum Bayesian approach to circuit QED measurement. Preprint at <http://arxiv.org/abs/1111.4016> (2011).
39. Korotkov, A. N. Quantum Bayesian approach to circuit QED measurement with moderate bandwidth. *Phys. Rev. A* **94**, 042326 (2016).
40. Pang, S. & Jordan, A. N. Optimal adaptive control for quantum metrology with time-dependent Hamiltonians. *Nat. Commun.* **8**, 14695 (2017).
41. Atalaya, J., Bahrami, M., Pryadko, L. P. & Korotkov, A. N. Bacon-Shor code with continuous measurement of noncommuting operators. *Phys. Rev. A* **95**, 032317 (2017).
42. Chantasri, A. & Jordan, A. N. Stochastic path-integral formalism for continuous quantum measurement. *Phys. Rev. A* **92**, 032125 (2015).
43. Clerk, A. A., Devoret, M. H., Girvin, S. M., Marquardt, F. & Schoelkopf, R. J. Introduction to quantum noise, measurement, and amplification. *Rev. Mod. Phys.* **82**, 1155 (2010).
44. Korotkov, A. N. Output spectrum of a detector measuring quantum oscillations. *Phys. Rev. B* **63**, 085312 (2001).
45. Korotkov, A. N. Persistent Rabi oscillations probed via low-frequency noise correlation. *Phys. Rev. B* **83**, 041406 (2011).
46. Atalaya, J., Hacothen-Gourgy, S., Martin, L. S., Siddiqi, I. & Korotkov, A. N. Multitime correlators in continuous measurement of qubit observables. *Phys. Rev. A* **97**, 020104(R) (2018).



Open Access This article is licensed under a Creative Commons Attribution 4.0 International License, which permits use, sharing, adaptation, distribution and reproduction in any medium or format, as long as you give appropriate credit to the original author(s) and the source, provide a link to the Creative Commons license, and indicate if changes were made. The images or other third party material in this article are included in the article's Creative Commons license, unless indicated otherwise in a credit line to the material. If material is not included in the article's Creative Commons license and your intended use is not permitted by statutory regulation or exceeds the permitted use, you will need to obtain permission directly from the copyright holder. To view a copy of this license, visit <http://creativecommons.org/licenses/by/4.0/>.

© The Author(s) 2018